Applied Radiation and Isotopes 197 (2023) 110798

Contents lists available at ScienceDirect

Applied Radiation and Isotopes

journal homepage: www.elsevier.com/locate/apradiso

Production and characterization of ^{111}Ag radioisotope for medical use in a TRIGA Mark II nuclear research reactor

L. Morselli [a,b], A. Donzella [c,d,*], A. Arzenton [a,e], M. Asti [f], S. Bortolussi [g,d], S. Corradetti [a], G. D'Agostino [h], M. Di Luzio [h], M. Ferrari [i,j], A. Gandini [k], M. Lunardon [l,m], V. Villa [c,d], A. Salvini [k], L. Zangrando [m], A. Zenoni [c,d], A. Andrighetto [a]

[a] INFN, Laboratori Nazionali di Legnaro, Viale dell'Università 2, 35020 Legnaro, Padua, Italy
[b] Dipartimento di Fisica e Scienze della Terra, Università degli Studi di Ferrara, Via G. Saragat 1, 44121 Ferrara, Italy
[c] Dipartimento di Ingegneria Meccanica e Industriale, Università degli Studi di Brescia, Via Branze 38, 25123 Brescia, Italy
[d] INFN, Sezione di Pavia, Via A. Bassi 6, 27100 Pavia, Italy
[e] Dipartimento di Scienze Fisiche della Terra e dell'Ambiente, Università degli Studi di Siena, Via Roma 56, 53100 Siena, Italy
[f] Radiopharmaceutical Chemistry Section, Nuclear Medicine Unit, AUSL-IRCCS di Reggio Emilia, Viale Risorgimento 80, 42122 Reggio Emilia, Italy
[g] Dipartimento di Fisica, Università degli Studi di Pavia, Via A. Bassi 6, 27100 Pavia, Italy
[h] Istituto Nazionale di Ricerca Metrologica, Dipartimento di Chimica Generale, Università degli Studi di Pavia, Viale T. Taramelli 12, 27100 Pavia, Italy
[i] Laboratoire Hubert Curien, CNRS, UMR 5516, Université Jean Monnet, F-42000, Saint-Etienne, France
[j] CERN, CH 1211 Geneva 23, Switzerland
[k] Laboratorio per l'Energia Nucleare Applicata, via G. Aselli 41, 27100 Pavia, Italy
[l] Dipartimento di Fisica ed Astronomia, Università degli Studi di Padova, Via F. Marzolo 8, 35131 Padova, Italy
[m] INFN, Sezione di Padova, Via F. Marzolo 8, 35131 Padova, Italy

ARTICLE INFO

Keywords:
ISOLPHARM project
Radiopharmaceuticals
^{111}Ag
γ-spectroscopy
Nuclear reactor

ABSTRACT

Radio Pharmaceutical Therapy (RPT) comes forth as a promising technique to treat a wide range of tumors while ensuring low collateral damage to nearby healthy tissues. This kind of cancer therapy exploits the radiation following the decay of a specific radionuclide to deliver a lethal dose to tumor tissues. In the framework of the ISOLPHARM project of INFN, ^{111}Ag was recently proposed as a promising core of a therapeutic radiopharmaceutical. In this paper, the production of ^{111}Ag via neutron activation of ^{110}Pd-enriched samples inside a TRIGA Mark II nuclear research reactor is studied. The radioisotope production is modeled using two different Monte Carlo codes (MCNPX and PHITS) and a stand-alone inventory calculation code FISPACT-II, with different cross section data libraries. The whole process is simulated starting from an MCNP6-based reactor model producing the neutron spectrum and flux in the selected irradiation facility. Moreover, a cost-effective, robust and easy-to-use spectroscopic system, based on a Lanthanum Bromo-Chloride (LBC) inorganic scintillator, is designed and characterized, with the aim of using it, in the future, for the quality control of the ISOLPHARM irradiated targets at the SPES facility of the Legnaro National Laboratories of INFN. ^{nat}Pd and ^{110}Pd-enriched samples are irradiated in the reactor main irradiation facility and spectroscopically characterized using the LBC-based setup and a multiple-fit analysis procedure. Experimental results are compared with theoretical predictions of the developed models, showing that inaccuracies in the available cross section libraries prevent an accurate reproduction of the generated radioisotope activities. Nevertheless, models are normalized to our experimental data allowing for a reliable planning of the ^{111}Ag production in a TRIGA Mark II reactor.

1. Introduction

Neutron-rich radioisotopes that decay through β^- decay are among the most used agents in Radio Pharmaceutical Therapy (RPT), and their production using nuclear reactors is a well established technique (Mirzadeh et al., 2011). Over the years, several radioisotopes were proposed as promising candidates for RPT, based on their decay characteristic (i.e. radiation type, released energy and half-life) and on the feasibility of their production.

* Corresponding author at: Dipartimento di Ingegneria Meccanica e Industriale, Università degli Studi di Brescia, Via Branze 38, 25123 Brescia, Italy.
E-mail address: antonietta.donzella@unibs.it (A. Donzella).

https://doi.org/10.1016/j.apradiso.2023.110798
Received 9 January 2023; Received in revised form 17 March 2023; Accepted 29 March 2023
Available online 30 March 2023
0969-8043/© 2023 Elsevier Ltd. All rights reserved.

When radioisotopes are produced for medical purposes (i.e. when they are used to prepare radiopharmaceuticals) a paramount feature of the preparation is a high molar activity, as non-radioactive isotopes of the sought radionuclide can compete with it for a finite number of cellular receptors.

A promising approach for producing high-specific activity, no-carrier-added radioisotopes is offered by the Isotope Separation On-Line (ISOL) technique (Dos Santos Augusto et al., 2014). In this context, the ISOLPHARM project aims to study innovative radioisotopes produced through ISOL techniques at SPES (Andrighetto et al., 2019) and, in particular, to investigate the preparation of ^{111}Ag-labeled radiopharmaceuticals (Ballan et al., 2020).

^{111}Ag is a β^- emitter with an half-life of 7.45 days and contemporary emission of two γ-rays (E_γ = 245.40(2) keV, I_γ = 1.24(9)%; E_γ = 342.13(2) keV, I_γ = 6.7(3)%) which potentially allow for SPECT imaging. Moreover, in the framework of RTP, the emission of a β^- having average energy of 360 keV makes it suitable for treating medium size tumors (Schubiger and Smith, 1995; Vértes et al., 2003). Finally, ^{111}Ag can be produced at SPES with good yields (Monetti et al., 2015).

In the framework of the ISOLPHARM project, since the SPES ISOL facility is currently under construction, preclinical experimentation of ^{111}Ag-based innovative radiopharmaceuticals will be carried out using ^{111}Ag produced via the radiative neutron capture reaction at the TRIGA Mark II nuclear research reactor of the LENA Laboratory of the University of Pavia (Italy) (Prata et al., 2014):

$$^{110}\mathrm{Pd}(n,\gamma)^{111}\mathrm{Pd} \xrightarrow{\beta^-} {}^{111}\mathrm{Ag} \tag{1}$$

This reaction can lead to the formation of ^{111}Pd in both its ground and metastable states depending on the distribution of resonance states produced in the process and the γ-multiplicity (Krane, 2019). In Fig. 1 a scheme of the different paths leading from ^{110}Pd to ^{111}Ag is reported, with the indication of the production rates, branching ratios and branching fractions. The ground and metastable states of ^{111}Pd have different half-lives, respectively 23.3 min for ^{111g}Pd and 5.5 h for ^{111m}Pd.

The time-evolution of the involved nuclides can be described by the following system of ordinary differential equations:

$$\begin{cases} \frac{dN_{\text{Pd-111m}}}{dt} = -\lambda_{\text{Pd-111m}} N_{\text{Pd-111m}} + PR_m N_{\text{Pd-110}} \\ \frac{dN_{\text{Pd-111g}}}{dt} = -\lambda_{\text{Pd-111g}} N_{\text{Pd-111g}} + BR_0^{\text{IT}} \lambda_{\text{Pd-111m}} N_{\text{Pd-111m}} + PR_g N_{\text{Pd-110}} \\ \frac{dN_{\text{Ag-111m}}}{dt} = -\lambda_{\text{Ag-111m}} N_{\text{Ag-111m}} + BF_1^{\beta-} \lambda_{\text{Pd-111g}} N_{\text{Pd-111g}} \\ \quad + BF_2^{\beta-} \lambda_{\text{Pd-111m}} N_{\text{Pd-111m}} \\ \frac{dN_{\text{Ag-111g}}}{dt} = -\lambda_{\text{Ag-111g}} N_{\text{Ag-111g}} \\ \quad + BF_0^{\beta-} \lambda_{\text{Pd-111g}} N_{\text{Pd-111g}} \\ \quad + BR_1^{\text{IT}} \lambda_{\text{Ag-111m}} N_{\text{Ag-111m}} \end{cases} \tag{2}$$

where λ_X is the decay constant and N_X is the number of nuclides of the X species, PR_g and PR_m are the production rates per target atom of the ground and metastable states of ^{111}Pd, BR_0^{IT} and BR_1^{IT} are the branching ratios of the isomeric gamma transitions of ^{111m}Pd to ^{111g}Pd and of ^{111m}Ag to ^{111g}Ag respectively, and $BF_0^{\beta-}$, $BF_1^{\beta-}$ and $BF_2^{\beta-}$ are the branching fractions for the production of the different daughter radionuclides by β-decay.

As recently reported (Krane, 2019), the neutron capture cross-section of ^{110}Pd favors the production of ^{111g}Pd over ^{111m}Pd. In that study, reference values of the isomer ratios in ^{111}Pd for thermal and epithermal neutrons are respectively: $R_{\text{th}} = 0.0385 \pm 0.0034$ and $R_{\text{epi}} = 0.0437 \pm 0.0046$. Following that result, we have assumed in this work that the values of PR_g and PR_m in Eq. (2) are constrained in such a way that the ratio $PR_m/(PR_g + PR_m)$, that is the ratio between the formation of the radioactive isomer and the total production of ^{111}Pd, is fixed to 4.0%.

In this paper, we present a study on the production and characterization of the ^{111}Ag radioisotope in a TRIGA Mark II nuclear research reactor, for its utilization in the ISOLPHARM research activities on innovative radiopharmaceuticals. This work follows several other studies performed in the past on the production of radioisotopes for medical use in research reactors (Deilami-nezhad et al., 2016; Hosseini et al., 2016, 2017; Karimi et al., 2019a,b; Sadeghi et al., 2019).

In the present study, a cost-effective spectroscopic system capable of characterizing the produced isotope is designed, constructed and tested. Thanks to its characteristics of robustness, low cost, reliability and ease of use, the realized detection system could also be used for applications in the harsh radiation environment of the SPES secondary target, where the produced radioisotope beams will be collected (Ballan et al., 2021).

The paper is organized as follows. In Section 2, the modeling of the production of the ^{111}Ag radioisotope in the TRIGA Mark II nuclear reactor is described, including the procedures for the calibration of the neutron flux in the reactor irradiation facility and the Monte Carlo simulation of the ^{nat}Pd and ^{110}Pd-enriched sample irradiation. In Section 3, the sample irradiation procedure, the experimental set-up, the characterization and calibration of the new realized detector are described.

In Section 4, the experimental results are shown and compared with the Monte Carlo simulations of the sample irradiation process, to validate the calculations. Predictions on the possibility of producing the ^{111}Ag radioisotope in the TRIGA Mark II nuclear reactor for ISOLPHARM research activities are illustrated. In Section 5, conclusions are drawn.

2. Modeling the production of ^{111}Ag in a TRIGA Mark II nuclear reactor

2.1. Modeling the irradiation facility

The TRIGA Mark II nuclear research reactor operating in Pavia is a 250 kW pool-type research reactor fueled with 20% enriched ^{235}U, cooled and partly moderated with demineralized light water. The reproducibility of the reactor power is below 1%.

The reactor core is composed of ninety slots occupied by fuel elements, a neutron source and three control rods placed in five concentric rings around a central channel, 40 cm useful length and 26 mm diameter, used as main irradiation facility and called Central Thimble (CT). The total neutron flux in the CT is about 1.7×10^{13} n/(cm^2 s) at full power. The reactor core is surrounded by a graphite reflector (Prata et al., 2014).

A computational model of the TRIGA Mark II reactor was previously set-up for radiobiological studies performed in the Thermal Column (Bortolussi et al., 2018). For the present study an update was necessary, and it was accomplished by the Monte Carlo neutron transport code MCNP6 (Goorley, 2014). The new version of the TRIGA Mark II reactor model considers the re-shuffle of the fuel elements in the core (Chiesa et al., 2016), each with a corrected burnup, accounting for the functioning time of the reactor. Fig. 2 shows a cross-section of the geometrical model of the whole reactor (XZ vertical plane, left) and a cross-section of the reactor core with the fuel elements in the new configuration (XY horizontal plane, right).

Simulations were carried out using the KCODE instruction, which reproduces the fission in the core of the reactor, starting with an external source that models an initial sampling of neutrons in the fuel bars, and letting MCNP simulate the generation of neutrons. An analysis of the convergence was carried out, by turning down all the variance reduction, and using the behavior of the Shannon entropy as an indicator of the convergence. This parameter, as well as the keff value, were plotted as a function of the KCODE cycle (Brown, 2009). After verifying that the convergence was achieved after 200 cycles, this source was recorded in an external srctp file describing the distribution of neutrons due to fission, with 5×10^3 cycles, each with

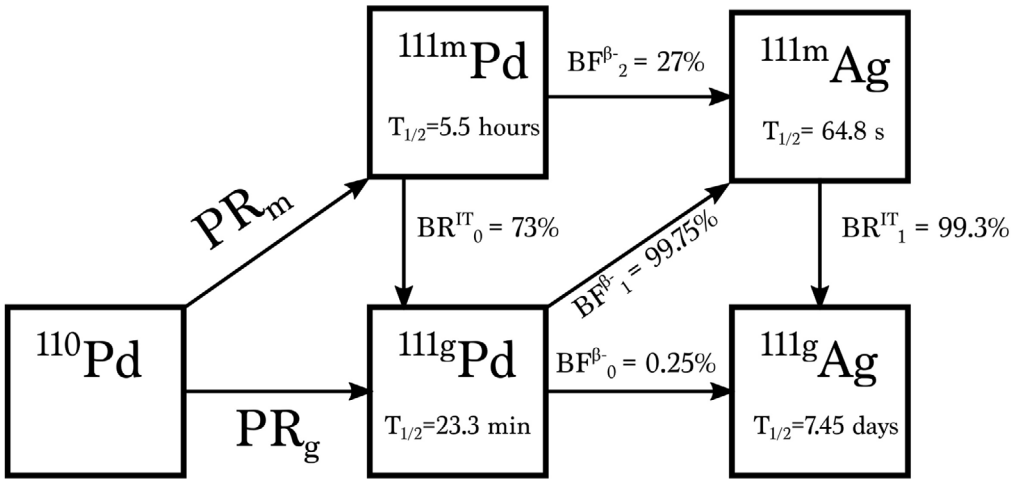

Fig. 1. Scheme of the different paths to produce ^{111g}Ag from neutron capture of ^{110}Pd (Krane, 2019). PR_g and PR_m are the production rates of ^{111g}Pd and ^{111m}Pd, respectivelly, per target atom; BR_0^{IT} and BR_1^{IT} are the branching ratios of the isomeric gamma transitions of ^{111m}Pd to ^{111g}Pd and ^{111m}Ag to ^{111g}Ag respectively; $BF_0^{\beta-}$, $BF_1^{\beta-}$ and $BF_2^{\beta-}$ are the branching fractions of the different beta-decays of ^{111g}Pd and ^{111m}Pd to ^{111g}Ag and ^{111m}Ag (Blachot, 2009).

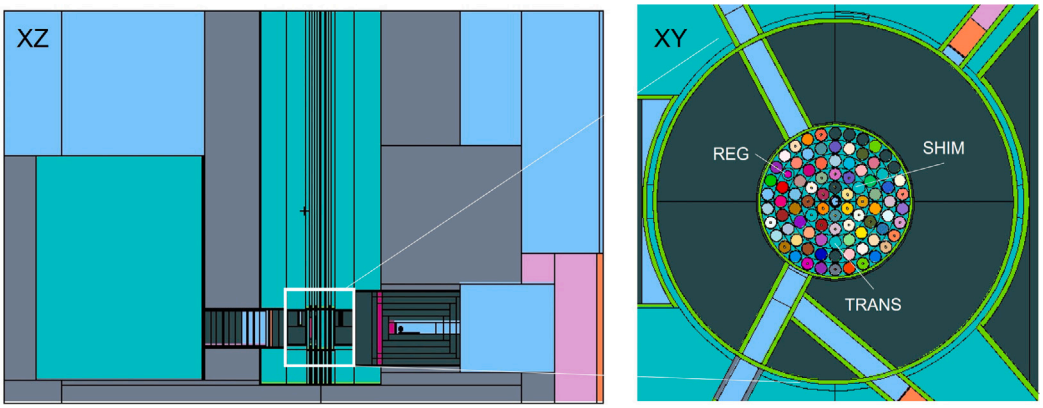

Fig. 2. Left: vertical cross-section of the reactor geometrical model, reproducing the whole structure of the TRIGA Mark II research reactor of the University of Pavia. Light blue: air, turquoise: water, gray: concrete, dark grey: graphite, purple: bismuth, pink: borated concrete. Right: horizontal cross-section of the reactor model showing the core with the fuel elements, the graphite reflector and the horizontal beam ports. Light green: aluminum. The core elements are represented in different colors each indicating a different composition of the fuel materials due to a different burnup. In the outer ring of fuel bars there are 5 dummy elements made of graphite. Two positions are void (turquoise) and correspond to the positions of two control bars which have been risen to obtain the criticality (trans and shim); the third bar (reg) is visible in the second ring on the left, partially extracted.

1×10^3 neutron/cycle. This file was used as input for the run of the tally calculations, to guarantee that the KCODE source takes as the initial distribution a robust neutron distribution that was proven to converge, and where the instruction ikz = 0 was specified. The criticality of the system was optimized adjusting the positions of the control bars. The final estimated combined collision/absorption/track-length keff was 1.00868, with an estimated standard deviation of 0.00004. The average number of neutrons produced per fission was 2.453.

The calculated neutron thermal flux in the CT was compared with the available flux measurements (Di Luzio et al., 2017, 2019), considered as a reference in the present study. Measurements were performed according to the Hogdahl convention (Høgdahl, 1962) using Zr and Au neutron flux monitor samples, placed at different positions along the CT. Conventional thermal Φ_T and epithermal Φ_E neutron flux values were obtained from the gamma spectra of the monitor samples. Gamma spectra were recorded with a HPGe detector, whose counting efficiency was determined using SI traceable gamma reference sources.

The measurement set-up was reproduced in the computational model including holder materials and inserts used to fix the positions of the samples. Fig. 3 shows the simulation of the CT where the set-up of the measurements (Di Luzio et al., 2017, 2019) has been reproduced including all the relevant materials (holders and activation targets).

The Φ_T value was calculated using the F4 tally type accounting for neutrons with energies below 0.56 eV. Fig. 4 shows the comparison between the reported experimental values and the results of the simulations. The relative error affecting the simulated Φ_T lies between −5% and +10% up to 25 cm from the bottom of the CT, and increases up to +38.5% at 34.5 cm.

To obtain the epithermal flux Φ_E from the simulated results, we used the expression (Di Luzio et al., 2017):

$$\phi_{epi}(E) = \frac{\Phi_E}{E^{1+\alpha}} \tag{3}$$

where $\phi_{epi}(E)$ is the energy distribution of the epithermal flux in the epithermal range and α is the parameter modeling the deviations from the $\frac{1}{E}$ theoretical trend.

For each monitor sample, we calculated the $\phi_{epi}(E)$ values from the neutron flux values Φ_{epi}, simulated with a BUGE-96 binning. The Φ_E value was calculated as the intercept of the straight line fitted to the $\log[\phi_{epi}(E)]$ vs. $\log(E)$ data, within the energy range comprised between 0.64 eV and 5.2×10^3 eV.

Fig. 5 shows the comparison between the reported experimental values and the results of the simulations. The simulated Φ_E values appear to be systematically overestimated relative to the experimental data.

The significant discrepancies affecting the simulated Φ_T at large distance from the CT bottom and the simulated Φ_E along all the CT

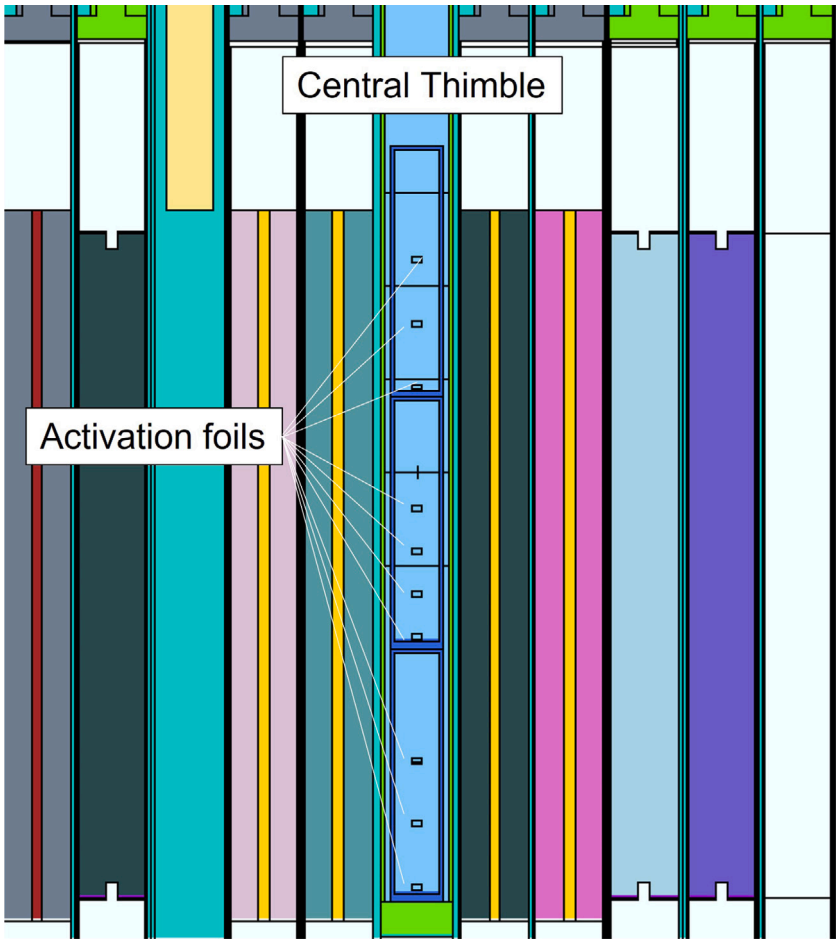

Fig. 3. Simulation of the CT where the measurement set-up (Di Luzio et al., 2017, 2019) has been reproduced including the polyethylene holders (royal blue) and the activation targets located at the same height where they were irradiated.

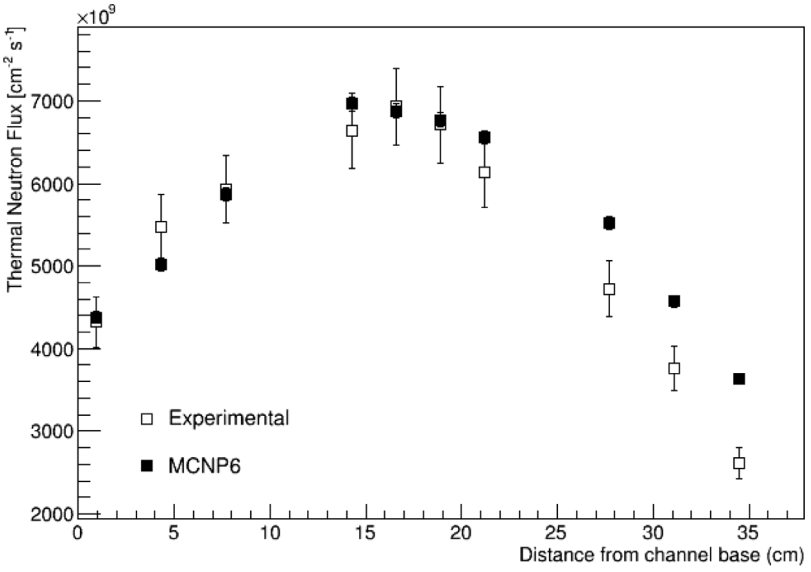

Fig. 4. Comparison between experimental thermal neutron flux values (empty squares) and Monte Carlo predictions (black filled squares) along the CT. Error bars of measured and simulated data indicate a 95% confidence interval.

required further investigations. They were mainly focused on the uncertainties affecting: the adoption of the Hogdahl convention; the modeling of dimensions and materials of the components; the calculation procedure to obtain Φ_T and Φ_E from the simulated data.

To test the actual performance of the model, we simulated both the ^{197}Au(n, γ)^{198}Au and ^{94}Zr(n, γ)^{95}Zr reaction rates per target nucleus, RR. Results were compared with experimental values recorded with Au and Zr samples (Di Luzio et al., 2017).

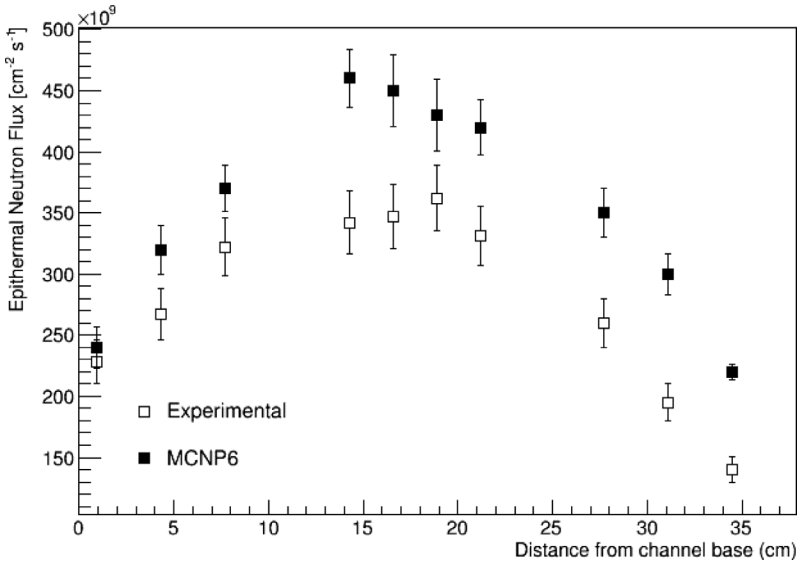

Fig. 5. Comparison between experimental epithermal neutron flux values (empty squares) and Monte Carlo predictions (black filled squares) along the CT. Error bars of measured and simulated data indicate a 95% confidence interval.

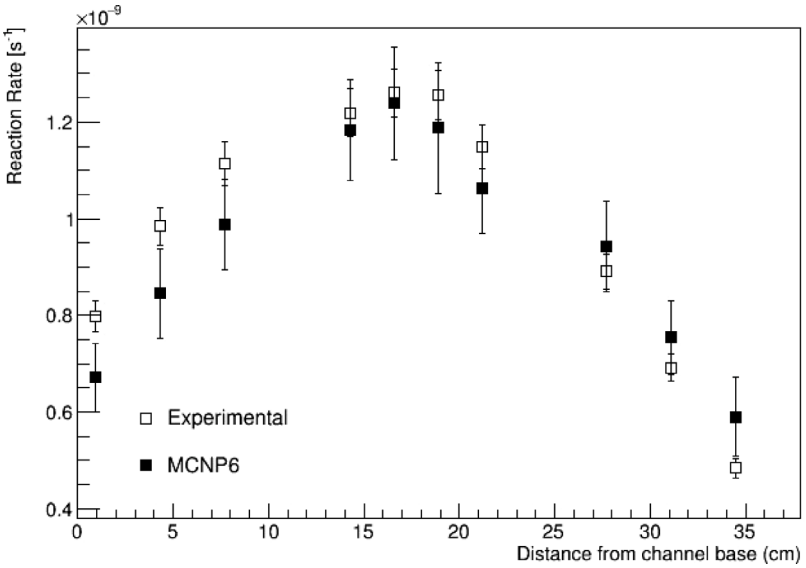

Fig. 6. Comparison between the experimental RR (empty squares) and simulated RR (filled black squares) for ^{197}Au(n, γ)^{198}Au in Au samples. Values are expressed per target nucleus; error bars of measured and simulated data indicate a 95% confidence interval.

It is worth noting that the reaction ^{110}Pd(n, γ)^{111}Pd has a resonance integral to thermal cross section ratio, Q_0, equal to 11.9, whereas the Q_0 values for ^{197}Au(n, γ)^{198}Au and ^{94}Zr(n, γ)^{95}Zr are 15.7 and 5.31, respectively. They are reported as recommended nuclear data in the k0 Data Base (database, 2020). In addition, based on the Hogdahl convention, RR can be expresses as:

$$RR = \Phi_T \sigma_0 [1 + \frac{Q_0(\alpha)}{f}] \quad (4)$$

where σ_0 is the thermal ($E = 2200$ m s^{-1}) neutron cross section, f is the conventional thermal to epithermal ratio Φ_T/Φ_E, and $Q_0(\alpha)$ is the ratio between the resonance integral and σ_0, for a $1/E^{(1+\alpha)}$ neutron spectrum in the epithermal region.

Accordingly, the contribution to RR due to the thermal and epithermal neutron flux for ^{110}Pd is close to the contribution for ^{197}Au and ^{94}Zr. Thus, the comparison carried out with ^{197}Au and ^{94}Z is meaningful to check the suitability of the computational model also for ^{110}Pd.

Results for the comparisons of experimental and simulated RR per target nucleus, for ^{197}Au and ^{94}Zr respectively, are shown in Figs. 6 and 7. RR are plotted versus the distance of the sample from the bottom of the CT.

The relative error affecting the simulated ^{197}Au RR values lies between −16.0%, at 0.9 cm from the bottom of the CT, and +23.0% at 34.5 cm. For the simulated ^{94}Zr RR values, it lies between −11.5% at 31.1 cm and +45.7% at 34.5 cm. In both cases, the best results are obtained close to the middle vertical position, for example at 14.3 cm, 16.6 cm, 18.9 cm and 21.2 cm from the bottom of the CT. In these positions, the relative error lies between −8.0% and +6.5%. Effects on RR of the significant discrepancies observed for Φ_E (see Fig. 5) are limited by the low percentage of epithermal neutron flux contributing to the reactions.

In conclusion, these results show that the updated TRIGA Mark II reactor model reproduces the thermal and epithermal neutron fluxes in a reliable way, in positions of the CT comprised between about 14 cm and 22 cm from the bottom of the CT, with an error less than 10%.

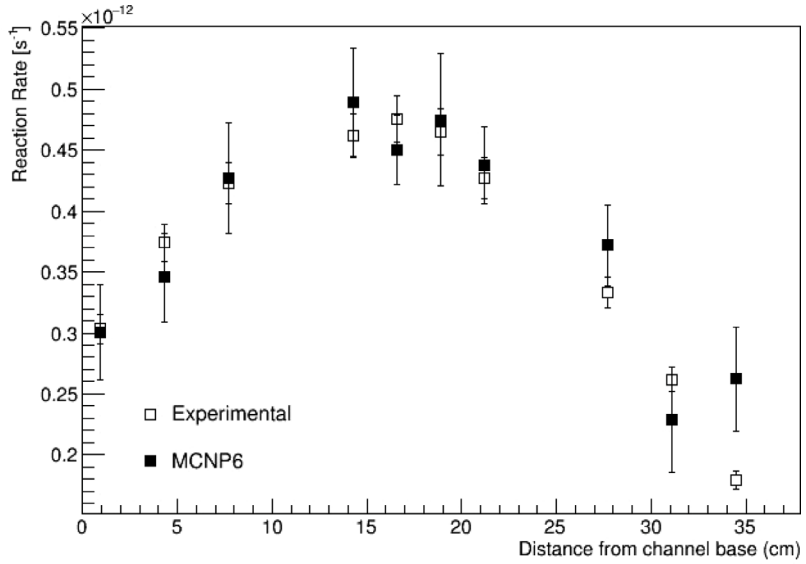

Fig. 7. Comparison between the experimental *RR* (empty squares) and simulated *RR* (filled black squares) for ^{94}Zr(n, γ)^{95}Zr in Zr samples. Values are expressed per target nucleus; error bars of measured and simulated data indicate a 95% confidence interval.

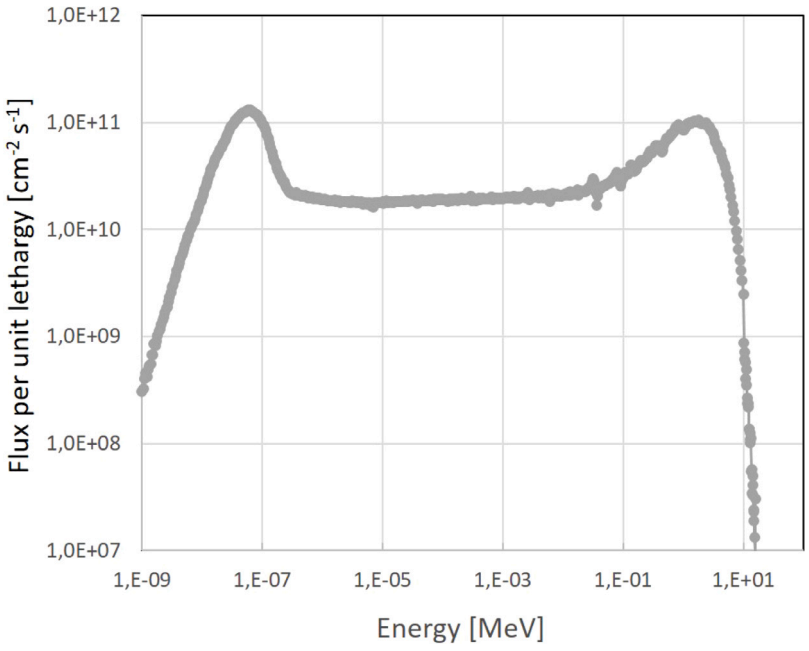

Fig. 8. Simulated neutron spectrum at about 17 cm from the bottom of the in the CT irradiation facility. The Monte Carlo statistical error is of the order of 1%.

In Fig. 8 the simulated neutron spectrum of the TRIGA Mark II reactor is shown. It includes the thermal, epithermal and fast components in the energy range between 1×10^{-9} MeV and 20 MeV, expressed in neutron/(cm^2 s^{-1}) per unit lethargy. The spectrum is calculated at the same position where the palladium samples are placed in the CT irradiation facility, at about 17 cm from the bottom of the CT. The spectrum is calculated in 709 group-energy bins with the described MCNP6 model of the reactor. In the following paragraph, this spectrum is used to model the palladium irradiation process with radioisotope formation and successive decays.

2.2. Modeling the palladium sample irradiation

Two Monte Carlo calculation tools, MCNPX (v2.7.0) (Pelowitz et al., 2011) and PHITS (v3.27) (Sato et al., 2018), are employed to model the irradiation of the palladium samples placed in the CT irradiation facility.

With both tools, a very simplified geometrical set-up is modeled, including a 100 mg palladium sample, the sample aluminum holder, the CT cylindrical cavity filled with air at NTP, surrounded by a cylindrical cell of the same size as the reactor core volume. Inside the latter volume, an isotropic neutron source with the same spectrum as the one reported in Fig. 8 is uniformly generated. Results of the simulation are normalized to the expected value of the neutron flux on the target holder at 250 kW reactor full power.

MCNPX and PHITS simulate the irradiation process and the isotope formation during the irradiation phase. To predict the radioisotope formation and decay at different times during the irradiation period and in the following cooling phase, MCNPX is interfaced with CINDER'90 (Gallmeier et al., 2010), a nuclide evolution program, whereas

Table 1
Isotopic composition of ^{nat}Pd and ^{110}Pd-enriched samples.

Isotope	^{nat}Pd	^{110}Pd-enriched
^{102}Pd	(1.02 ± 0.01)%	0.01%
^{104}Pd	(11.14 ± 0.08)%	0.05%
^{105}Pd	(22.33 ± 0.08)%	0.09%
^{106}Pd	(27.33 ± 0.03)%	0.13%
^{108}Pd	(26.46 ± 0.09)%	0.33%
^{110}Pd	(11.72 ± 0.09)%	(99.4 ± 0.10)%

PHITS makes use of the internal DCHAIN utility (Ratliff et al., 2020) to perform the same operation.

A supplementary calculation of the palladium sample activation, with subsequent nuclide evolution at different times, is performed with FISPACT-II (Sublet et al., 2017), a stand-alone enhanced multiphysics inventory code. Effective cross sections are built by weighting the average over energy of suitable cross-sections libraries, read in 709 bin group structure, on the neutron spectrum calculated in the CT with the MCNP6 model of the reactor reported in Fig. 8. Then, subsequent nuclide evolution at different time steps is performed, supposing constant irradiation conditions during each step and a homogeneous, infinite and infinitely diluted irradiated material.

To model the interactions of the low-energy neutrons produced by the reactor in the palladium samples and the time evolution of the generated radioisotopes, some different cross-section data libraries and decay data files are implemented in the simulation programs. Indeed, as discussed in Section 4, different libraries contain sometimes rather different cross section data for the same reactions or do not include cross sections for relevant metastable states.

Two types of palladium samples are considered in the simulations: ^{nat}Pd and ^{110}Pd-enriched samples. In the experimental part of this work, described in Section 3, both types of samples are irradiated.

^{nat}Pd samples are mainly used for testing the procedures of irradiation and characterization. ^{110}Pd-enriched samples are needed to maximize the ^{111}Ag production, reducing, at the same time, the production of the undesired ^{109}Pd radioisotope. Indeed, the latter is produced via neutron capture on the ^{108}Pd stable isotope and quickly decays into the stable isotope ^{109}Ag, impossible to be chemically separated from the desired ^{111}Ag. Therefore, if present in abundance, it may definitely compromise the specific activity of the produced ^{111}Ag.

The isotopic compositions of the ^{nat}Pd sample and of the ^{110}Pd-enriched sample are reported in Table 1.

3. Palladium irradiation and characterization

3.1. Palladium sample irradiation

The experiment is performed irradiating, at the same time and in the same polyethylene holder, a 62.7 mg ^{110}Pd-enriched and a 60.7 mg ^{nat}Pd sample. Both samples are irradiated for one hour inside the CT at the full reactor power of 250 kW. They are placed at about 17 cm from the CT bottom, approximately at the center of the reactor core.

After the end of the irradiation, the samples cool down for 2.5 h prior to the start of the spectroscopic measurements. The ^{110}Pd-enriched sample is measured for a total time of 21 h, splitting the whole measurement in 20-min long single batches (see Section 4.1). The ^{nat}Pd sample is measured only once for a period of 20 min, immediately after the end of the ^{110}Pd-enriched sample measurement.

The ^{nat}Pd sample is measured to perform a consistency check of the measurement procedure. In fact, the ratio between the measured activities of ^{111}Ag in the two samples, R_{Ag111}, must be equal to the ratio between the amounts of ^{110}Pd contained in the two samples, R_{Pd110}.

3.2. Experimental setup

The samples are characterized using a spectroscopic system designed for the quality control of the ISOLPHARM collection target system at the SPES facility (Ballan et al., 2021). The requirements of the designed detector system are the following:

- to be able to sustain high acquisition rates with negligible dead time, since high activities are expected;
- to have a good energy resolution (e.g. between 3% and 4% at 661 keV) allowing for a reliable spectroscopic characterization of the samples;
- to be compact, portable and easy to use; indeed, it is intended to be also used in experimental activities correlated with the ISOLPHARM project (i.e. ex-vivo bio-distribution studies (Tosato et al., 2022)).

The proposed system is based on a Lanthanum Bromo-Chloride (LBC) inorganic scintillation detector. The choice represents a cost-effective solution with respect to the standard use of HPGe detectors. Indeed, considering its aim, the high energy resolution (at least ten times better than inorganic scintillators) is not mandatory, since only isobaric beams will be deposited onto the aforementioned collection targets and thus the acquired γ-spectra should be populated by only a few separated peaks. This crystal exhibits an intrinsic background, similar to the one of the Lanthanum Bromide ($LaBr_3$) detectors (Gilmore, 2008), which does not represent a concern for high count rate measurements.

The selected LBC crystal, manufactured by SCIONIX, has a fast anode signal (about 100 ns) and dead time effects are negligible below 50 kHz. It presents a cylindrical shape, with 1 inch (2.54 cm) diameter and 1 inch height, encapsulated in a dedicated aluminum case due to the crystal hygroscopicity. The crystal is coupled with a R6231 PMT having a superbialkali photo-cathode manufactured by HAMAMATSU. The whole assembly is enclosed in a custom designed plastic case realized using plastic additive manufacturing. Since irradiated samples are transported inside a 3 mL plastic vial, a dedicated support is also designed in order to ensure a well defined distance between the detector and the sample to be measured (see Fig. 9a).

To provide an additional check on the characterization and calibration of the new LBC detector, the same ^{110}Pd-enriched sample, irradiated in the same conditions in a different experiment, was measured using an HPGe detector. The adopted REGe™detector is an n-type Reverse Electrode Germanium detector manufactured by Mirion Technologies. The spectroscopic measurement started 16 h after the end of the irradiation.

The PMT anode signal is digitized using a CAEN DT-5725 digitizer, while the PMT voltage (operated at −650 V) is supplied using an USB powered desktop HV power supply manufactured by CAEN (DT-5470). The Digital Pulse Processing (DPP) firmware is flashed on the digitizer FPGA which provided on-line, for each event, the relative time-stamp alongside the complete integration of the signal (Long Gate). The average duration of the LBC pulses is 100 ns. The digitizer has a sampling frequency of 250 MHz with 14 bit resolution. The Long Gate was set to 30 samples (=120 ns).

In order to enhance the energy resolution of the setup, the relevant DPP parameters are optimized making it possible to reach an energy resolution of 3.08% at 661.6 keV.

The acquisition is controlled using the ABCD (Acquisition and Broadcast of Collected Data) open source software (Fontana et al., 2017, 2018).

The detector absolute full energy peak efficiency is evaluated through a Monte Carlo simulation of the detector implemented using the GEANT4 toolkit (Agostinelli et al., 2003). The whole detector geometry is built in GEANT4 starting from the CAD design drawings using the CADMesh library (Poole et al., 2012) (see Fig. 9b). The

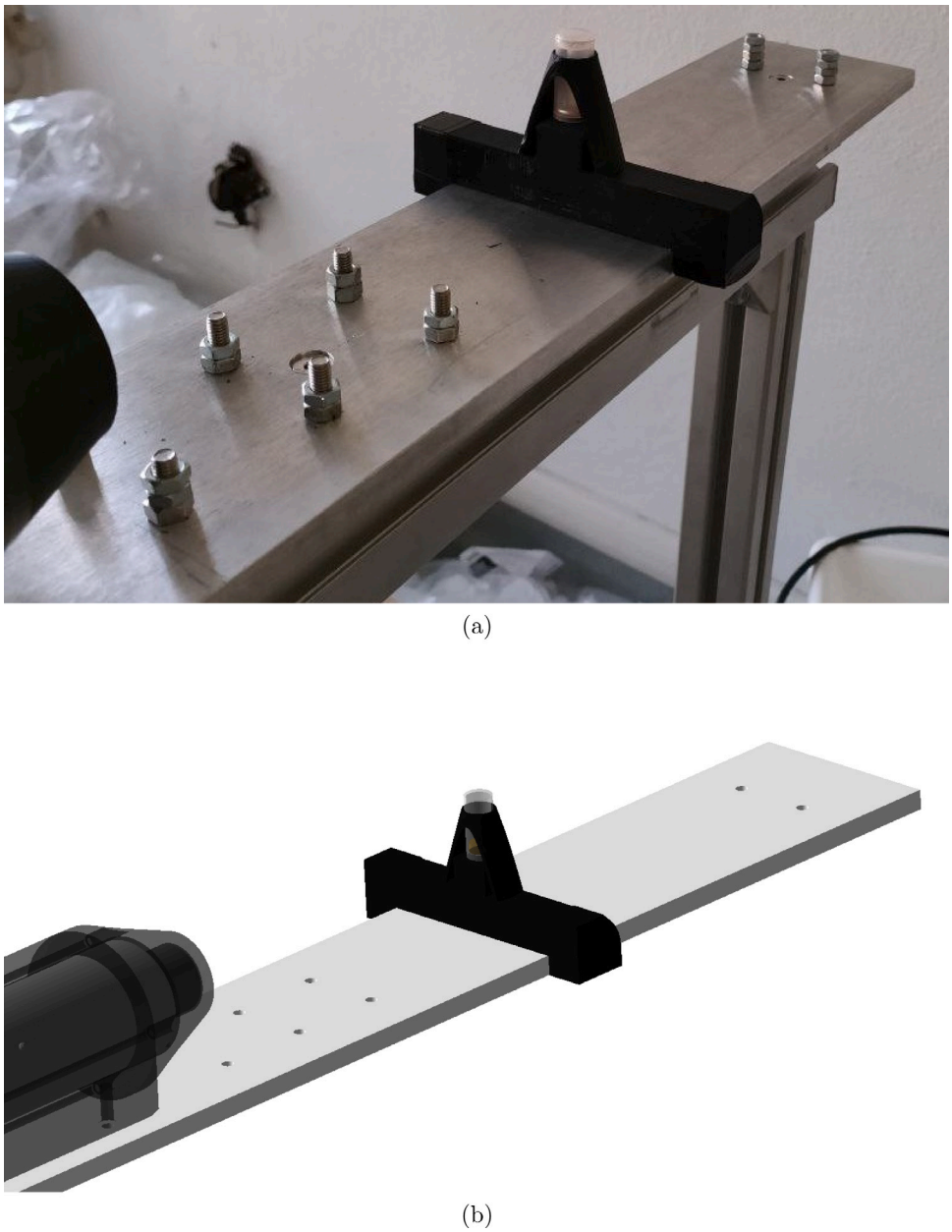

Fig. 9. Comparison between (a) a picture of the experimental setup and (b) the GEANT4 simulation geometry.

simulation is validated with measurements using ^{60}Co, ^{133}Ba, ^{137}Cs, ^{152}Eu and ^{241}Am γ-calibration sources.

The graph of Fig. 10 shows a good agreement above 200 keV and up to 1.5 MeV between the experimental values of efficiency and the MC simulation. Below this threshold, the experimental efficiency appears to be overestimated by the MC simulations; this may be due to discrepancies between the actual geometry and the one reported in the manufacturer datasheet used for the simulation. However, for the present study, only efficiencies above 200 keV are required.

All the simulations were run by means of the CloudVeneto private Cloud infrastructure (Andreetto et al., 2020).

4. Results

4.1. Mesurement of ^{111}Ag and ^{111m}Pd activities

In Fig. 11, the γ-ray spectra obtained from a 20-min measurement of a ^{nat}Pd sample and a ^{110}Pd-enriched one are shown. The measurements are performed 5 h after the end of the irradiation.

As expected, the γ-rays associated with the decay of ^{111}Ag are more evident in the spectrum taken with the ^{110}Pd-enriched sample, given the larger amount of ^{110}Pd contained. In the following, we focus on the data collected with the ^{110}Pd-enriched sample and on two γ transitions of the produced radioisotopes: 342 keV for ^{111}Ag and 391 keV for ^{111m}Pd respectively.

The activity A, in Bequerel, extrapolated from a specific gamma transition, is obtained from the relation:

$$A = \frac{N}{\varepsilon \cdot I_\gamma \cdot T} \tag{5}$$

where N is the number of counts under the peak associated to a given transition, ε is the absolute detection efficiency, I_γ is the gamma intensity of the transition and T is the acquisition time in seconds.

To obtain the number of events N associated with a specific transition during a given time T, data are split into 20-min long batches from which energy spectra are obtained. From each spectrum, the environmental plus intrinsic background is subtracted using a long acquisition without any sample.

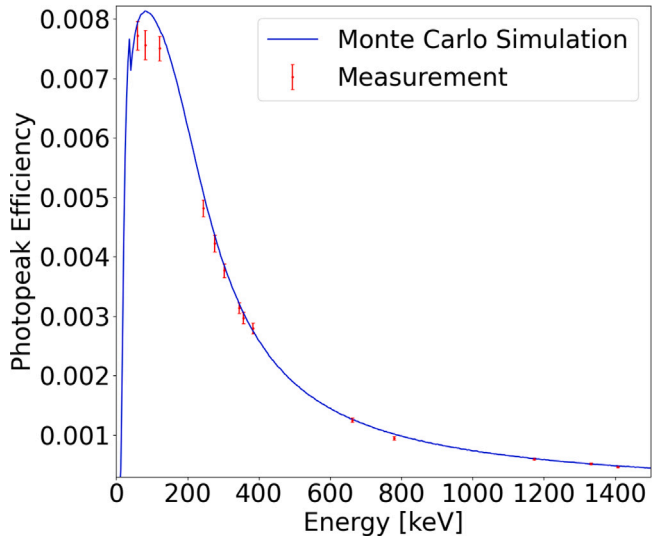

Fig. 10. Absolute full energy peak efficiency of the LBC detector estimated by experiments and MC simulations.

Table 2
List of all the γ peaks considered in the multiple fit procedure (Blachot, 2009; Kumar et al., 2016). In bold character the two γ transitions studied.

Nuclide	E_i [keV]	I_γ [%]
^{109}Pd	309	0.00424 ± 0.00013
	311	0.0338 ± 0.0009
	413	0.00718 ± 0.00021
	415	0.0114 ± 0.0003
^{111m}Pd	309	0.00424 ± 0.00013
	358	0.44 ± 0.06
	376	0.92 ± 0.15
	391	**5.7 ± 0.7**
	413	1.9 ± 0.5
	415	1.7 ± 0.4
	439	0.25 ± 0.05
	444	0.132 ± 0.019
	454	0.27 ± 0.11
^{111}Ag	**342**	**6.7 ± 0.3**

Due to the great number of transition peaks present in the spectra and the limited energy resolution of the LBC detector, a fit procedure considering only a single peak plus exponential background at a time, turns out to be rather ineffective and unstable.

For this reason, a simultaneous multiple fit procedure on the full spectrum is adopted. In Table 2, the list of the main γ transition energies and intensities present in the measured spectra, in the region of interest between 290 keV and 500 keV, is shown. Data are taken from NDS (Blachot, 2009; Kumar et al., 2016).

Each subtracted spectrum is fitted, between 290 keV and 500 keV, with the following formula:

$$f(E) = ae^{-bE} + \sum_{E_i \in \{E_1,\ldots,E_n\}} \frac{A_{E_i}}{\sqrt{2\pi}\sigma_{E_i}} e^{-\frac{1}{2}\left(\frac{E-E_i}{\sigma_{E_i}}\right)^2} \tag{6}$$

where E_i are the peak energies, A_{E_i} are the peak areas in the spectrum and σ_{E_i} are the standard deviations associated to the energy broadening of the peaks due to the LBC scintillator energy resolution. The exponential term represents the physical background in the spectrum measurement, where a and b are free parameters.

In order to reduce the degrees of freedom of the function, the fit is done by fixing all the peak energies within the fitting region at the values reported in Table 2. The standard deviation of the 342 keV peak is left as a free parameter, while the standard deviations of the all the other peaks are appropriately scaled using the following relation:

$$\sigma(E_i) = \sigma_{342} \cdot \sqrt{\frac{E_i}{E_{342}}} \tag{7}$$

Since the estimation of the background term is largely reliant on the fit energy limits, the fit is repeated a number of times for each spectrum by systematically varying the minimum and maximum energy limits. The obtained distributions of the free parameters allowed the systematic error associated with the fit technique to be estimated as the standard deviations of the distributions themselves.

Energy spectra from 20-min long data batches collected at different times after the end of the irradiation are analyzed with the described procedure. The result of the multiple fits of the spectra allowed the values of the peak areas A_{E_i} to be extracted at different times for the two γ transitions under study: 342 keV for ^{111}Ag and 391 keV for ^{111m}Pd respectively. From the peak areas the contained number of events N is extracted and the ^{111}Ag and ^{111m}Pd activities are calculated at different times with Eq. (5).

The experimental results are reported in Fig. 12, where the activities of the two analyzed isotopes, measured with the LBC detector, are reported at different times after the beginning of the irradiation. The error bars account both for the statistical error and for the systematic error. The latter is due mainly to the uncertainty on the intensities of the gamma transitions in Table 2 and to the systematic error in the aforementioned multiple fit procedure. In the same plot, the isotope activities measured with the HPGe detector in another equivalent experiment, for the same ^{110}Pd-enriched sample, are reported too. The latter measurements started 16 h after the end of the irradiation. The solid lines are the solution of the system of ordinary differential equations of Eq. (2) with $PR_m/(PR_g + PR_m) = 4.0\%$.

From Fig. 12 some conclusions can be drawn. First, the absolute value of the ^{111}Ag and ^{111m}Pd activities measured with the LBC detector, using the simultaneous multiple fit procedure, and with the HPGE detector are in very good agreement. This confirms the accuracy of the LBC detector calibration and characterization and the effectiveness of the analysis procedure.

Second, the measured yields of ^{111m}Pd and ^{111}Ag are compatible with the isomer ratios between the metastable and the ground states of ^{111}Pd (Krane, 2019). Indeed, the solution of the system of Eq. (2) is calculated with the ratio $PR_m/(PR_g + PR_m)$ constrained to 4.0% and is normalized on the measured yields of ^{111}Ag. The measured activities of ^{111m}Pd are slightly below the theoretical predictions that are anyway contained inside the systematic error. The last is mainly due to the uncertainty on the intensities of the gamma transitions in Table 2.

The curves interpolate correctly the data also at short times after the beginning of the irradiation, where the balance of the ground and metastable states of ^{111}Pd, which have very different half-lives, manifests itself in the data behavior. Moreover, the measured exponential decays of the two radioisotopes ^{111}Ag and ^{111m}Pd are well in agreement with the reference half-lives, 7.45 days and 5.5 h, respectively.

Finally, it is demonstrated that the irradiation of a ^{110}Pd-enriched sample of 62.7 mg during one hour in the TRIGA Mark II reactor CT, at full power, can produce 122 ± 5 μCi of ^{111}Ag and 110 ± 13 μCi of ^{111m}Pd, 3.5 h after the beginning of the irradiation. This result allows a reliable planning of the ^{111}Ag production for the use in the ISOLPHARM project to be performed.

4.2. Measurement of the ^{110}Pd isotopic ratio

As reported in Section 3.1, the ^{nat}Pd sample is irradiated and measured to check the consistency of the measurement and of the analysis procedures. In fact, the ratio between the measured activities of ^{111}Ag in the ^{nat}Pd and ^{110}Pd-enriched samples, R_{Ag111}, must be equal to the ratio between the amounts of ^{110}Pd contained in the two samples, R_{Pd110}.

Indeed, the measured value $R_{Ag111} = (11.7 \pm 0.5)\%$ is found to be compatible with the reference $R_{Pd110} = (11.8 \pm 0.14)\%$ obtained by Table 1.

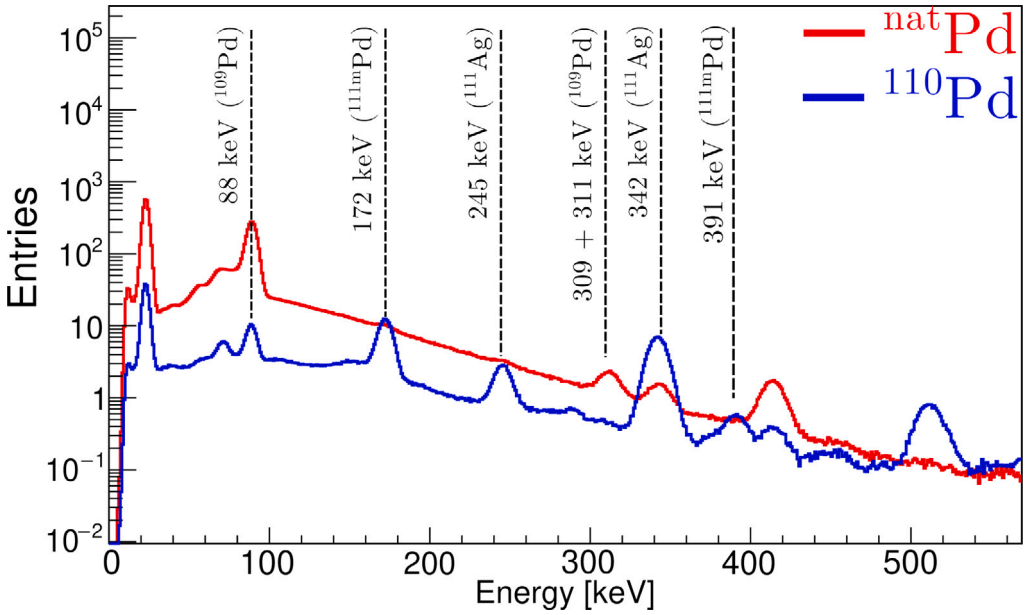

Fig. 11. γ-ray spectra of the irradiated ^{nat}Pd and ^{110}Pd-enriched samples, obtained from a 20-min measurement after 5 h from the end of the irradiation.

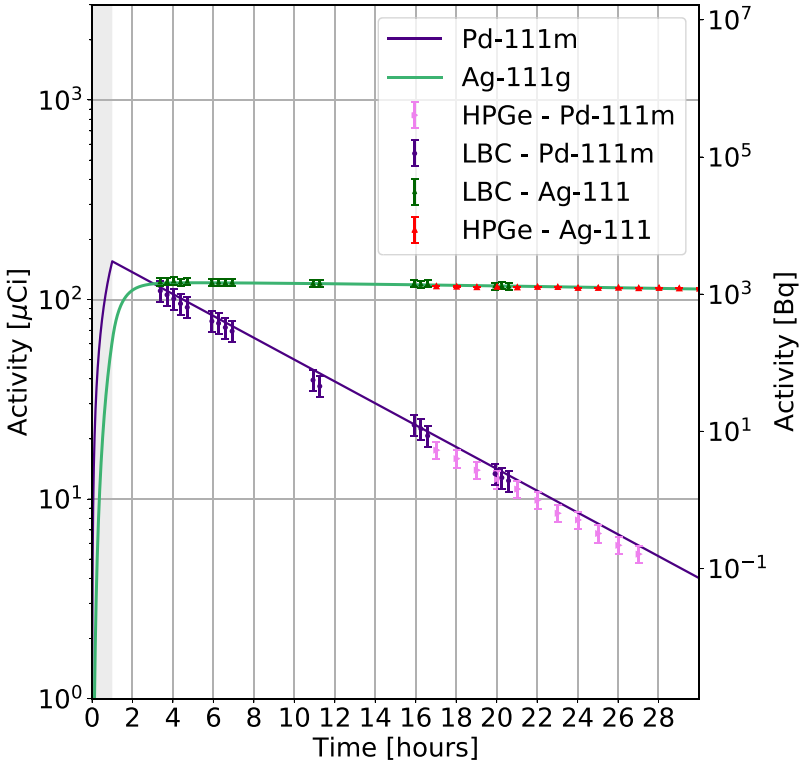

Fig. 12. Activities of ^{111}Ag, measured with LBC (green) and HPGe (red), and of ^{111m}Pd, measured with LBC (purple) and HPGe (pink), at different times after the beginning of the irradiation. The solid lines are the solution of the system of ordinary differential equations of Eq. (2) with $PR_m/(PR_g + PR_m) = 4.0\%$.

4.3. Comparison with model predictions

The present experimental results are compared with the predictions obtained with the model of the palladium sample irradiation process described in Section 2. In Fig. 13, the activity of ^{111}Ag, measured both with LBC and HPGe detectors as a function of the elapsed time after the beginning of the irradiation, is compared with the predictions of Monte Carlo simulations. Experimental and theoretical values are normalized to a 100 mg ^{110}Pd-enriched sample.

As illustrated in Section 2, simulations of the process are performed with MCNPX and PHITS. In addition, a calculation of the ^{111}Ag produced activity is performed with the inventory simulation code FISPACT-II. The neutron flux in the CT calculated by the updated model of the TRIGA Mark II reactor, and shown in Fig. 8, is used. All calculations are performed with different sets of cross section libraries. From Figs. 4, 6 and 7, the systematic error associated to the modeling of the neutron flux is estimated to be less than 10%.

Fig. 13 shows that no combination of calculation tool and cross section library reproduces satisfactorily the absolute values of the

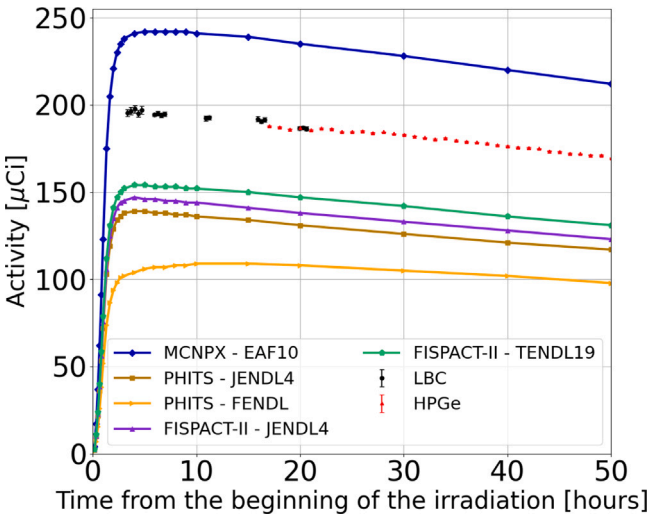

Fig. 13. Comparison between measured ^{111}Ag activity, normalized to a ^{110}Pd-enriched sample of 100 mg irradiated for one hour in the CT of the TRIGA Mark II reactor, and Monte Carlo simulations with different tools and cross section libraries. Monte Carlo statistical uncertainties are lower than 5%.

experimental data. Data are indeed positioned between the theoretical predictions of MCNPX with EAF-2010 and CINDER'90 data library (blue curve) (+25%), and PHITS with JENDL-4.0 (brown curve) (−40%) and FENDL/A-3.0 (orange curve) (−70%). Moreover, theoretical predictions of PHITS with FENDL/A-3.0 do not reproduce the data behavior at short times after the beginning of the irradiation, where the balance of the ground and metastable states of ^{111}Pd determines the slope of the curve.

The use of the same calculation tool with different cross section libraries, as PHITS with JENDL-4.0 and FENDL/A-3.0, produces predictions with large differences. Conversely, the use of the same cross section library, JENDL-4.0, with different calculation tools as PHITS and FISPACT-II (violet curve) produces comparable predictions. Finally, FISPACT-II with the TENDL-2019 cross section libraries (green curve), provides the best approximation to the experimental data.

Hence, we can conclude that the disagreement between the different model predictions and the experimental data is likely due to inaccuracies in the available cross section libraries for the ^{110}Pd$(n,\gamma)^{111}$Pd reaction. Nevertheless, based on the presented results, the predictions of the model can be normalized to the experimental data in order to plan with a sufficient confidence the ^{111}Ag production in the TRIGA Mark II reactor for use in the ISOLPHARM project activities.

4.4. Prediction of the ^{111}Ag production at the TRIGA Mark II reactor

In Fig. 14, the prediction of the activities of three generated radioisotopes, ^{111g}Pd (green curve), ^{111m}Pd (violet curve) and ^{111}Ag (red curve) is shown. They are produced in a three-day irradiation of a 100 mg ^{110}Pd-enriched sample in the CT of the TRIGA Mark II reactor at full power. The activities are plotted as a function of the time after the beginning of the irradiation. A duty cycle of the TRIGA Mark II reactor of 6 h irradiation a day is assumed, compatible with the LENA laboratory standard operations, during three days.

Calculations are performed using FISPACT-II with the TENDL-2019 cross section library. In agreement with the results of Section 4.3, this combination of tools provides the best approximation to the experimental data. Moreover, TENDL-2019 is the most recent and most complete cross section library available. Theoretical predictions should underestimate the effective ^{111}Ag production by about 25%.

For these reasons, we can reasonably expect that the production of ^{111}Ag by irradiation of ^{110}Pd-enriched samples in the TRIGA Mark II reactor may amount to an average of 1 mCi per day per 100 mg of irradiated ^{110}Pd-enriched material during a few days. Over several irradiation periods, the cumulated inventory of ^{111}Ag, whose half-life is 7.45 days, also accounts for the decay of the ^{111}Ag nuclides but it globally increases by steps of 1 mCi over successive periods.

5. Conclusion

In the present paper, a study of the production and characterization of ^{111}Ag radioisotope for medical use in a TRIGA Mark II nuclear research reactor, via the neutron capture reaction on ^{110}Pd (see Eq. (1)), has been performed. The model of the TRIGA Mark II reactor of the LENA laboratory of the University of Pavia, Italy, was updated to match experimental data on the measured neutron flux in the reactor CT irradiation facility.

A new detection system based on a Lantanum Bromo-Cloride (LBC) inorganic scintillator was designed and constructed. The detection system features high acquisition rate, sufficient energy resolution, compactness, portability, and ease to use. It is a robust and cost-effective solution with respect to the standard represented by high resolution HPGe detectors. The new LBC-based detector system has been successfully tested by measuring the spectra of ^{nat}Pd and ^{110}Pd-enriched samples after one hour irradiation in the reactor.

A model of the sample irradiation process was developed by means of MCNPX, PHITS and FISPACT-II calculation tools, and different cross

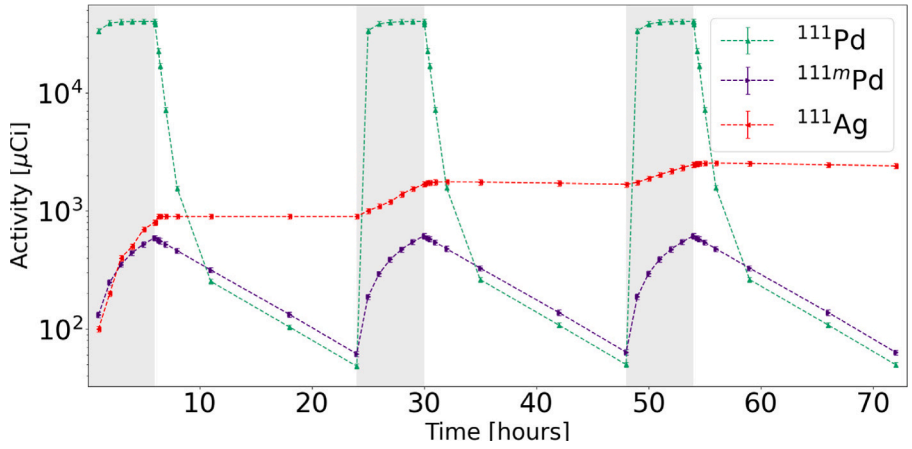

Fig. 14. Activities of ^{111}Pd, ^{111m}Pd and ^{111}Ag, produced irradiating a 100 mg ^{110}Pd-enriched sample in the CT of the TRIGA Mark II reactor at full power. Activities are plotted as a function of time after the beginning of the irradiation. A duty cycle of the TRIGA Mark II reactor of 6 h a day is assumed. Irradiation periods are highlighted in grey. Calculations are performed using FISPACT-II with the TENDL-2019 cross section library. Monte Carlo statistical uncertainties are lower than 5%.

section libraries. Comparison of the experimental results obtained with the predictions of the models shows that inaccuracies in the cross-section libraries of the above mentioned production reaction prevent the accurate reproduction of the experimental values of the produced ^{111}Ag activity.

Nevertheless, model predictions can be normalized to the obtained experimental values, in view to estimate the production of the ^{111}Ag isotope in the TRIGA Mark II reactor, with the aim of testing innovative radiopharmaceuticals based on ^{111}Ag in the ISOLPHARM project.

CRediT authorship contribution statement

L. Morselli: Writing – original draft, Validation, Software, Methodology, Investigation, Formal analysis, Data curation, Conceptualization. **A. Donzella:** Writing – original draft, Software, Methodology, Investigation, Formal analysis, Conceptualization. **A. Arzenton:** Software, Investigation, Data curation. **M. Asti:** Investigation, Data curation, Conceptualization. **S. Bortolussi:** Writing – original draft, Software, Methodology, Conceptualization. **S. Corradetti:** Visualization, Project administration. **G. D'Agostino:** Writing – original draft, Methodology, Conceptualization. **M. Di Luzio:** Writing – original draft, Methodology, Conceptualization. **M. Ferrari:** Software, Conceptualization. **A. Gandini:** Methodology, Investigation, Data curation. **M. Lunardon:** Writing – original draft, Software, Methodology, Investigation, Data curation, Conceptualization. **V. Villa:** Conceptualization. **A. Salvini:** Methodology, Data curation, Conceptualization. **L. Zangrando:** Software, Data curation. **A. Zenoni:** Writing – original draft, Validation, Methodology, Investigation, Formal analysis, Conceptualization. **A. Andrighetto:** Validation, Supervision, Resources, Project administration, Conceptualization.

Declaration of competing interest

The authors declare that they have no known competing financial interests or personal relationships that could have appeared to influence the work reported in this paper.

Data availability

Data will be made available on request.

Acknowledgments

This research was carried out in the framework of the ISOLPHARM_EIRA experiment, supported by INFN, aimed at the design and characterization of innovative radiopharmaceuticals based on the ^{111}Ag radioisotope.

References

Agostinelli, S., Allison, J., Amako, K.a., Apostolakis, J., Araujo, H., Arce, P., Asai, M., Axen, D., Banerjee, S., Barrand, G., et al., 2003. GEANT4—a simulation toolkit. Nucl. Instrum. Methods Phys. Res. A 506 (3), 250–303. http://dx.doi.org/10.1016/S0168-9002(03)01368-8.

Andreetto, P., Costa, F., Crescente, A., Fantinel, S., Fanzago, F., Mazzon, P.E., Menguzzato, M., Sella, G., Sgaravatto, M., Traldi, S., et al., 2020. Evolution of the CloudVeneto. it private cloud to support research and innovation. In: EPJ Web of Conferences, Vol. 245. EDP Sciences, p. 07013. http://dx.doi.org/10.1051/epjconf/202024507013.

Andrighetto, A., Tosato, M., Ballan, M., Corradetti, S., Borgna, F., Di Marco, V., Marzaro, G., Realdon, N., 2019. The ISOLPHARM project: ISOL-based production of radionuclides for medical applications. J. Radioanal. Nucl. Chem. 322 (1), 73–77. http://dx.doi.org/10.1007/s10967-019-06698-0.

Ballan, M., Tosato, M., Verona, M., Caeran, M., Borgna, F., Vettorato, E., Corradetti, S., Zangrando, L., Sgaravatto, M., Verlato, M., et al., 2020. Preliminary evaluation of the production of non-carrier added 111Ag as core of a therapeutic radiopharmaceutical in the framework of ISOLPHARM_Ag experiment. Appl. Radiat. Isot. 164, 109258. http://dx.doi.org/10.1016/j.apradiso.2020.109258.

Ballan, M., Vettorato, E., Morselli, L., Tosato, M., Nardella, S., Borgna, F., Corradetti, S., Monetti, A., Lunardon, M., Zenoni, A., et al., 2021. Development of implantation substrates for the collection of radionuclides of medical interest produced via ISOL technique at INFN-LNL. Appl. Radiat. Isot. 175, 109795. http://dx.doi.org/10.1016/j.apradiso.2021.109795.

Blachot, J., 2009. Nuclear data sheets for A=111. Nucl. Data Sheets 110, 1239–1407. http://dx.doi.org/10.1016/j.nds.2009.04.002.

Bortolussi, S., Protti, N., Ferrari, M., Postuma, I., Fatemi, S., Prata, M., Ballarini, F., Carante, M., Farias, R., González, S., Marrale, M., Gallo, S., Bartolotta, A., Iacoviello, G., Nigg, D., Altieri, S., 2018. Neutron flux and gamma dose measurement in the BNCT irradiation facility at the TRIGA reactor of the University of Pavia. Nucl. Instrum. Methods Phys. Res. B 414, 113–120. http://dx.doi.org/10.1016/j.nimb.2017.10.023.

Brown, F., 2009. A Review of Best Practices for Monte Carlo Criticality Calculations. Los Alamos National Laboratory, Los Alamos, NM, LA-UR-09-03136.

Chiesa, D., Clemenza, M., Pozzi, S., Previtali, E., Sisti, M., Alloni, D., Magrotti, G., Manera, S., Prata, M., Salvini, A., Cammi, A., Zanetti, M., Sartori, A., 2016. Fuel burnup analysis of the TRIGA Mark II reactor at the University of Pavia. Ann. Nucl. Energy 96, 270–276. http://dx.doi.org/10.1016/j.anucene.2016.06.008.

database, K., 2020. Nuclear data SC data base. URL: http://www.kayzero.com/k0naa/k0naaorg/Nuclear_Data_SC/Nuclear_Data_SC.html.

Deilami-nezhad, L., Moghaddam-Banaem, L., Sadeghi, M., Asgari, M., 2016. Production and purification of Scandium-47: A potential radioisotope for cancer theranostics. Appl. Radiat. Isot. 118, 124–130. http://dx.doi.org/10.1016/j.apradiso.2016.09.004.

Di Luzio, M., D'Agostino, G., Oddone, M., Salvini, A., 2019. Vertical variations of flux parameters in irradiation channels at the TRIGA Mark II reactor of Pavia. Prog. Nucl. Energy 113, 247–254. http://dx.doi.org/10.1016/j.pnucene.2019.01.025.

Di Luzio, M., Oddone, M., Prata, M., Alloni, D., D'Agostino, G., 2017. Measurement of the neutron flux parameters f and α at the Pavia TRIGA Mark II reactor. J. Radioanal. Nucl. Chem. 312 (1), 75–80. http://dx.doi.org/10.1007/s10967-017-5191-4.

Dos Santos Augusto, R.M., Buehler, L., Lawson, Z., Marzari, S., Stachura, M., Stora, T., collaboration, C.-M., et al., 2014. CERN-MEDICIS (medical isotopes collected from ISOLDE): a new facility. Appl. Sci. 4 (2), 265–281. http://dx.doi.org/10.3390/app4020265.

Fontana, C.L., Carnera, A., Lunardon, M., Pino, F.E., Sada, C., Soramel, F., Stevanato, L., Moretto, S., 2018. A distributed data acquisition system for nuclear detectors. In: International Journal of Modern Physics: Conference Series, Vol. 48. World Scientific, 1860118. http://dx.doi.org/10.1142/S2010194518601187.

Fontana, C.L., Lunardon, M., Pino, F.E., Stevanato, L., Carnera, A., Sada, C., Soramel, F., Moretto, S., 2017. A distributed data acquisition system for signal digitizers with on-line analysis capabilities. In: 2017 IEEE Nuclear Science Symposium and Medical Imaging Conference (NSS/MIC). IEEE, pp. 1–5. http://dx.doi.org/10.1109/NSSMIC.2017.8533063.

Gallmeier, F.X., Ferguson, P.D., Lu, W., Iverson, E.B., Muhrer, G., Holloway, S.T., Kelsey, C., Pitcher, E., Wohlmuther, M., Micklich, B.J., 2010. The CINDER'90 transmutation code package for use in accelerator applications in combination with MCNPX. URL: https://www.osti.gov/biblio/1027400.

Gilmore, G., 2008. Practical Gamma-Ray Spectroscopy. John Wiley & Sons.

Goorley, T., 2014. MCNP6. 1.1-Beta Release Notes. Technical Report. LA-UR-14-24680.

Høgdahl, T., 1962. Neutron Absorbtion in Pile Neutron Analysis. Technical Report. MMPP-226-1.

Hosseini, S.F., Sadeghi, M., Aboudzadeh, M.R., 2017. Theoretical assessment and targeted modeling of TiO2 in reactor towards the scandium radioisotopes estimation. Appl. Radiat. Isot. 127, 116–121. http://dx.doi.org/10.1016/j.apradiso.2017.05.016.

Hosseini, S.F., Sadeghi, M., Aboudzadeh, M.R., Mohseni, M., 2016. Production and modeling of radioactive gold nanoparticles in Tehran research reactor. Appl. Radiat. Isot. 118, 361–365. http://dx.doi.org/10.1016/j.apradiso.2016.10.004.

Karimi, Z., Sadeghi, M., Ezati, A., 2019a. Modeling and experimental production yield of 64Cu with natCu and natCu-NPs in Tehran Research Reactor. Nucl. Eng. Technol. 51 (1), 269–274. http://dx.doi.org/10.1016/j.net.2018.08.008.

Karimi, Z., Sadeghi, M., Hosseini, S.F., 2019b. Experimental production and theoretical assessment of 67Cu via neutron induced reaction. Ann. Nucl. Energy 133, 665–668. http://dx.doi.org/10.1016/j.anucene.2019.07.012.

Krane, K., 2019. Neutron capture cross sections of Pd 108, 110. Phys. Rev. C 99 (4), 044313. http://dx.doi.org/10.1103/PhysRevC.99.044313.

Kumar, S., Chen, J., Kondev, F., 2016. Nuclear data sheets for A=109. Nucl. Data Sheets 137, 1–286. http://dx.doi.org/10.1016/j.nds.2016.09.001.

Mirzadeh, S., Mausner, L., Garland, M.A., 2011. Reactor-produced medical radionuclides. In: Handbook of Nuclear Chemistry. p. 1857. http://dx.doi.org/10.1007/978-1-4419-0720-2-38.

Monetti, A., Andrighetto, A., Petrovich, C., Manzolaro, M., Corradetti, S., Scarpa, D., Rossetto, F., Dominguez, F.M., Vasquez, J., Rossignoli, M., et al., 2015. The RIB production target for the SPES project. Eur. Phys. J. A 51 (10), 1–11. http://dx.doi.org/10.1140/epja/i2015-15128-6.

Pelowitz, D.B., Durkee, J.W., Elson, J.S., Fensin, M.L., Hendricks, J.S., James, M.R., Johns, R.C., McKinney, G.W., Mashnik, S.G., Verbeke, J.M., et al., 2011. MCNPX 2.7. 0 Extensions, Vol. 4. Los Alamos National Laboratory, Los Alamos, NM, http://dx.doi.org/10.2172/1058045, LA-UR-11-02295.

Poole, C.M., Cornelius, I., Trapp, J.V., Langton, C.M., 2012. A CAD interface for GEANT4. Australas. Phys. Eng. Sci. Med. http://dx.doi.org/10.1007/s13246-012-0159-8.

Prata, M., Alloni, D., De Felice, P., Palomba, M., Pietropaolo, A., Pillon, M., Quintieri, L., Santagata, A., Valente, P., 2014. Italian neutron sources. Eur. Phys. J. Plus 129 (11), 1–15. http://dx.doi.org/10.1140/epjp/i2014-14255-3.

Ratliff, H.N., Matsuda, N., ichiro Abe, S., Miura, T., Furuta, T., Iwamoto, Y., Sato, T., 2020. Modernization of the DCHAIN-PHITS activation code with new features and updated data libraries. Nucl. Instrum. Methods Phys. Res. B 484, 29–41. http://dx.doi.org/10.1016/j.nimb.2020.10.005.

Sadeghi, M., Aboudzadeh Rovais, M.R., Zandi, N., Moradi, M., Yousefi, K., 2019. Production assessment of non-carrier-added 199Au by (n,gamma) reaction. Appl. Radiat. Isot. 154, 108877. http://dx.doi.org/10.1016/j.apradiso.2019.108877.

Sato, T., Iwamoto, Y., Hashimoto, S., Ogawa, T., Furuta, T., Abe, S.-i., Kai, T., Tsai, P.-E., Matsuda, N., Iwase, H., Shigyo, N., Sihver, L., Niita, K., 2018. Features of Particle and Heavy Ion Transport code System(PHITS) version 3.02. J. Nucl. Sci. Technol. 55 (6), 684–690. http://dx.doi.org/10.1080/00223131.2017.1419890.

Schubiger, P.A., Smith, A., 1995. Optimising the radioimmunotherapy of malignant disease: the broadening choice of carrier and effector moieties. Pharm. Acta Helv. 70 (3), 203–217. http://dx.doi.org/10.1016/0031-6865(95)00013-y.

Sublet, J.-C., Eastwood, J., Morgan, J., Gilbert, M., Fleming, M., Arter, W., 2017. FISPACT-II: an advanced simulation system for activation, transmutation and material modelling. Nucl. Data Sheets 139, 77–137. http://dx.doi.org/10.1016/j.nds.2017.01.002.

Tosato, M., Verona, M., Favaretto, C., Pometti, M., Zanoni, G., Scopelliti, F., Cammarata, F.P., Morselli, L., Talip, Z., van der Meulen, N.P., et al., 2022. Chelation of theranostic copper radioisotopes with S-rich macrocycles: From radiolabelling of copper-64 to in vivo investigation. Molecules 27 (13), 4158. http://dx.doi.org/10.3390/molecules27134158.

Vértes, A., Nagy, S., Klencsár, Z., Lovas, R.G., Rösch, F., 2003. Handbook of Nuclear Chemistry, Vol. 4. Springer.